FERMILAB-PUB-10-377-TD

Routine characterization of 3-D profiles of SRF cavity defects using replica techniques

M Ge, G Wu, D Burk, J Ozelis, E Harms, D Sergatskov, D Hicks, and L D Cooley
Fermi National Accelerator Laboratory, PO Box 500, Batavia IL 60510, USA.

E-mail: mingqi@fnal.gov

Abstract. Recent coordination of thermometry with optical images has shown that obvious defects at specific locations produce heat or even quench superconducting radio frequency (SRF) cavities, imposing a significant limit on the overall accelerating gradient produced by the cavity. Characterization of the topography at such locations provides clues about how the defects originated, from which schemes for their prevention might be devised. Topographic analyses also provide understanding of the electromagnetic mechanism by which defects limit cavity performance, from which viability of repair techniques might be assessed. In this article we discuss how a variety of two-component silicone-based room-temperature vulcanizing agents can be routinely used to make replicas of the cavity surface and extract topographic details of cavity defects. Previously, this level of detail could only be obtained by cutting suspect regions from the cavity, thus destroying the cavity. We show 3-D profiles extracted from several different 1.3 GHz cavities. The defect locations, which were all near cavity welds, compelled us to develop extraction techniques for both equator and iris welds as well as from deep inside long 9-cell cavities. Profilometry scans of the replicas yield micrometer-scale information, and we describe various curious features, such as small peaks at the bottom of pits, which were not apparent in previous optical inspections. We also discuss contour information in terms of electromagnetic mechanisms proposed by others for local cavity heating. We show that production of the replica followed by high-pressure rinsing dose not adversely affect the cavity RF performance.

1. Introduction

Superconducting Radio-Frequency (SRF) technology has been widely used as the basis for the state of art accelerators. Compared to normal conducting technology, SRF cavities have many orders of magnitude higher intrinsic quality factor (Q_0) due to extremely low power loss on the cavity wall. Hence a SRF cavity is more economical than a copper cavity even after accounting for the refrigeration power needed to provide liquid helium. Another important advantage of SRF cavities is high accelerating gradient for operation in continuous wave (CW) and long-pulse modes. Thereby, such accelerators can be shorter and have less beam disruption, which dramatically benefits high-current applications.

Large numbers of SRF cavities are required for the large accelerator projects such as the International Linear Collider (ILC), Fermilab's Project X, and a potential muon collider. The ILC, for instance, needs over 16,000 1.3 GHz 9-cell SRF cavities, 90% of which must reach an accelerating electric-field gradient of 35 MV/m with a quality factor (Q_0) of 8×10^9 after their first-pass process and test cycle [1].

However, at present, less than 30% of the 9-cell cavities developed for the ILC achieved the target gradient after the initial standard surface preparation procedure [2]. As repeated processing and testing of SRF cavities represents a substantial additional cost to an accelerator project, reproducibility of cavity performance is a significant issue.

Superconducting cavities that achieve the highest levels of RF performance, >40MV/m in the best examples, benefit from extremely smooth surface [3, 4]. Yet, cavity processing is by no means perfect, and Surface defects such as pits, bumps, cracks, scratches, etc., have been identified as main contributors to the spread in accelerating gradient, which for ILC-type cavities extends down to 15 MV/m [2]. Uunderstanding why such defects formed is of utmost importance for devising manufacturing changes that might prevent defect formation. Also analyzing the details of these defects provides information from which the electromagnetic mechanisms of cavity performance limitation can be evaluated. Such detailed information also guides strategies to repair flaws by various techniques. When taken together, the beneficial consequences of analyzing defects in detail would be to increase the cavity performance reproducibility and come closer to the goals of large-scale high performance accelerator applications.

Optical inspection techniques have been developed for the identification and observation of surface defects by Kyoto University, Cornell University, KEK, Jefferson Lab, and Los Alamos National Lab [5]. At Fermilab, several optical inspection systems have been implemented. By using a high resolution CCD camera, vivid images of surface defects can be acquired without contacting the cavity surface. A defect's size and, more roughly, depth can be measured by adjusting the illumination of the optical system [5, 6]. Optical inspections of cavities have allowed correlations to be made between pits or other surface features and quench locations where there is local heating. The heating has been observed during cavity quenching in vertical test (measurement of Q_0 vs. accelerating gradient while placed in a Dewar filled with superfluid helium) by using the well-established technique of arrays of thermometers attached to the outside of the cavity surface (so-called T-mapping system) [7, 8].

Simulations indicate that the magnetic field is enhanced at the edge of a defect, which leads to localized heating when the cavity is being driven to high electric and magnetic fields. The enhancement factor depends on the sharpness of the defect edge [9]. When this enhanced magnetic field at the defect edge exceeds the local critical magnetic field, the edge transitions from the superconducting to the normal conducting state. This leads to a sudden increase in surface impedance. If this increase in surface impedance causes the cavity wall temperature to locally exceed the critical temperature, the entire cavity will quench [10, 11].

While this general picture provides guidance about the severity of allowable defects, and perhaps also explains why repeated processing increases performance by making more gradual rounding of defect edges, ref. [9] uses an ideal geometry model to estimate the defect shape. Real cavity pits have much more complicated geometry, with rich details that could be relevant. Therefore, extracting quantitative 3-D data that incorporates height, depth, width, edge radius and so on is very important to improve electromagnetic models. However, optical inspection techniques are not sufficiently capable of providing such so far.

In this article, we show how replica techniques have now evolved to the point where they can be widely applied to extract detailed topography of features and the surrounding region. The replica allows the cavity surface to be duplicated with micrometer accuracy. Scanning profilometry applied to the replica then digitally reproduces the 3-D profile of the cavity surface. It also allows surface topography, such as surface roughness, to be compared before and after different fabrication and processing steps. Replica techniques, therefore, appear to be a viable means to greatly improve the amount of detailed cavity surface data that can be obtained, which could tremendously improve the understanding of the materials science related to cavity surface preparation.

Before the development of replica techniques, suspect locations had to be cut out of the cavity in order to get quantitative data [12, 13]. Unfortunately, the need to sacrifice an expensive cavity through destructive evaluation techniques (cavities are made from high-purity niobium requiring a significant investment in fabrication and processing effort) has historically limited opportunities to pursue many materials studies.

2. Replica Technique

The original attempt to apply replica techniques to SRF cavities was performed by S. Berry, et al. [14, 15]. There are several technical concerns: Firstly the chosen replica material should be able to preserve the important details of the surface. Defects inside SRF cavities are typically 100-1000 μm in diameter and 10-100 μm in depth. Thus, the required resolution of replicas should be ~1 μm to keep uncertainty below 10%. The second concern is to safely deliver the moulding material into the target area and to extract it after curing, without damaging the interior surface of the 1.2 meters long 9-cell cavity whose beam pipe diameter is only 70 mm. The last, but most important concern is retention of cavity RF performance after applying mould and high-pressure ultrapure water rinsing (HPR). Choice of the material, curing, and application must ensure that most if not all residues left on the cavity surface can be removed by HPR, making the technique harmless to cavity RF performance.

2.1 Material choice

Replica materials can be resin, rubber, or plastic based; there are many choices such as Araldite SV40 (Speciality Chemicals), Microset 101 RF (Microset Products Ltd), and Technovit 3040 (Heraeus Kulzer GmbH) [16].

In this article, we prefer a two-component translucent silicone-based compound, Rhodorsil RTV-3040 (Freeman Mfg., Inc.). This material has extremely low linear shrinkage, less than 0.1%, and has high tensile strength, 6,343 KPa indicated by test method ASTM D412 [17]. The material properties imply an ability to preserve surface details as well as resist cracking and chipping when peeled out of a cavity. RTV-3040 cures at room temperature in 16 hours, and no release agent or baking is needed.

Before being used, the silicone must be degassed in a vacuum. This is a necessary step for achieving accurate reproduction of surface details, as the large quantity of air bubbles that are entrained in the material during the mixing process can attach to the surface being replicated and affect the resultant surface contour. After curing at room temperature, the mould is extracted from the cavity. An imprint (negative) of the surface is obtained. Subsequently, a low temperature epoxy (100 g Epon resin 828 with 50 g Shell Epi-Cure 3055, with 1 g carbon black and 1 drop of an anti-foaming agent added) is used to make a cast (positive) of the moulding material. The exact surface is duplicated after the epoxy cures, maintaining a dimensional accuracy of 1μm.

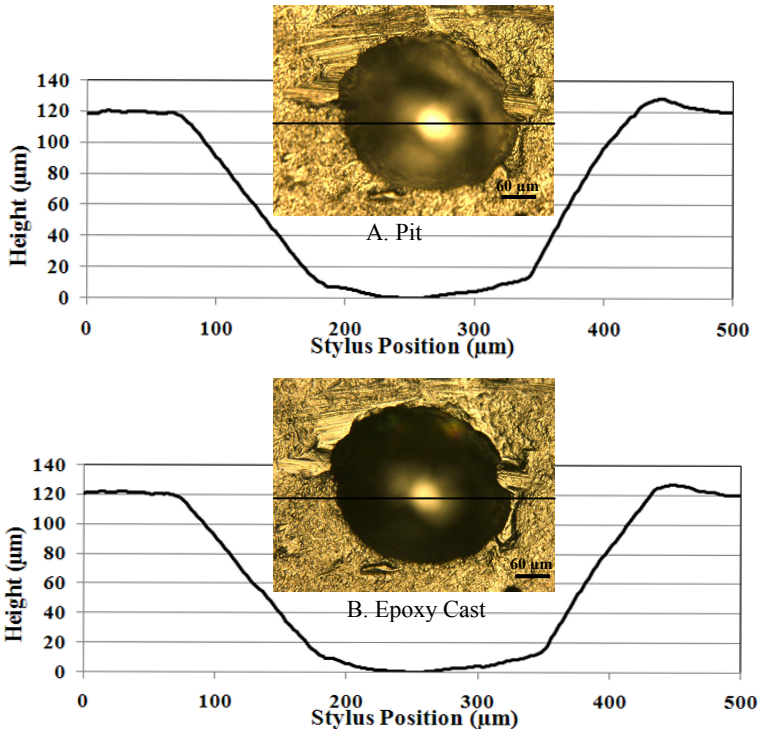

Figure 1. Light microscopy images and corresponding traces obtained using a stylus profilometer for an impression made by a simple punch tool into a niobium coupon. At top (A) is the actual impression, at bottom (B) is the result for an epoxy cast made from the silicone replica. The black lines across the photographs indicate the path of the stylus.

Figure 1 compares the images of an indentation made on a Nb coupon by a punch tool and its positive casting from the replica. Beneath each photo is a representative profile taken across the pit using a stylus profilometer (indicated by the line drawn across each photo). The pit size is about 125 μm deep and 300 μm in diameter. The nearly identical features and profiles demonstrate that the replica preserves the details of the pits, including the contour information and the surface morphology around the pit. The accuracy of the replica with the epoxy mould is about 1-2 μm after carefully comparing of profiles in Figure 1. This accuracy is evident in the profilometer traces. This level of accuracy is suitable for analyzing pits inside SRF cavities.

2.2 Extraction tool design

The engineering challenges for making replicas of features in an SRF cavity, especially for the inner cells of a 9-cell cavity, are to safely deliver the moulding material into the target area and to extract it after curing without damaging the interior surface of the cavity through inadvertent contact. An elaborate tool shown in

Figure 2a was developed. A cup holding liquid silicone is located in the head. It can reach any cell of a 9-cell cavity by moving the stage on the rail, and the arm can be rotated to pour the silicone after the head arrives above the region where a feature is located. The silicone is cured with a string encased inside, which is then used to pull the cured silicone out of cavity as shown in Figure 2b. A similar design has been concurrently developed at KEK [18].

In addition to the equator region, replicas can be made of the iris region of a 9-cell cavity. The iris replica requires the cavity to be placed in a vertical position. An inflated balloon can then be used as plug to allow the silicone to cover the iris while it is being cured, yet prevent it from escaping into other regions of the cavity interior. In this case the delivery of the silicone agent is straightforward by pouring down the cavity bore.

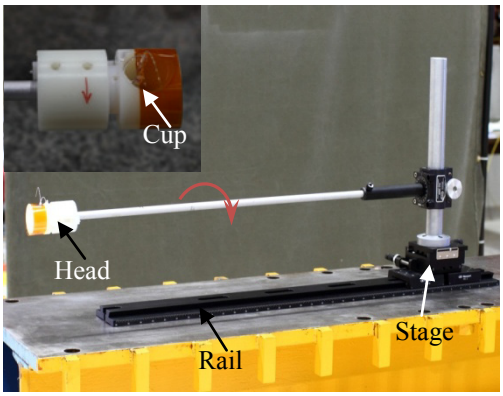

A. The image of a tool holding and pouring sililcone into cavity.

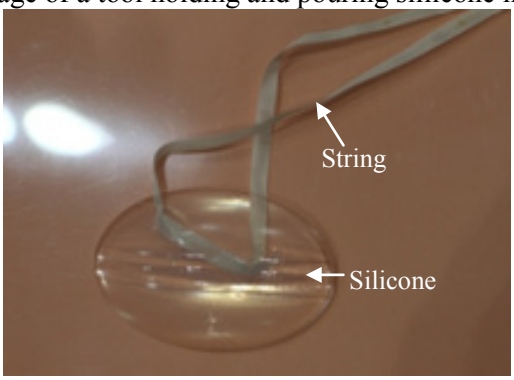

B. The silicone solidified with string after being pulled out of 9-cell cavity.

Figure 2. Replica material pouring tool developed at Fermilab. In (A) the inserted image is the magnified view of the head and cup.

2.3 No degradation of cavity RF performance

The molding material we chose was determined to present low risk for cavity RF performance. Its new compounds were designed to produce a mould that could be removed without the use of any release agents, which normally would be sprayed or somehow coated onto the area of interest. This was thought to be crucial to leave the surface unaltered. Samples exposed to the silicone rubber were analyzed by Auger Electron Spectroscopy, which showed no detectable traces of silicone rubber after peeling away the mould without rinsing.

Several RF tests of single-cell cavities were conducted to assure the cavity performance would not degrade after the moulding material was applied to them. All of these single cell cavities were rinsed with particle-free ethanol before receiving high pressure water rinsing. All of the cavity RF tests indicated that there was no performance degradation due to the application and removal of the moulding material. Figure 3, as an example, shows the performance comparison of cavity TE1AES004 before and after applying molding material. The RF performance after molding remains the same. It is interesting to see that, in the case of

cavity TE1AES004, there is actually somewhat higher Q_0 after molding than before. The cavity also remained free of field emission after the molding application.

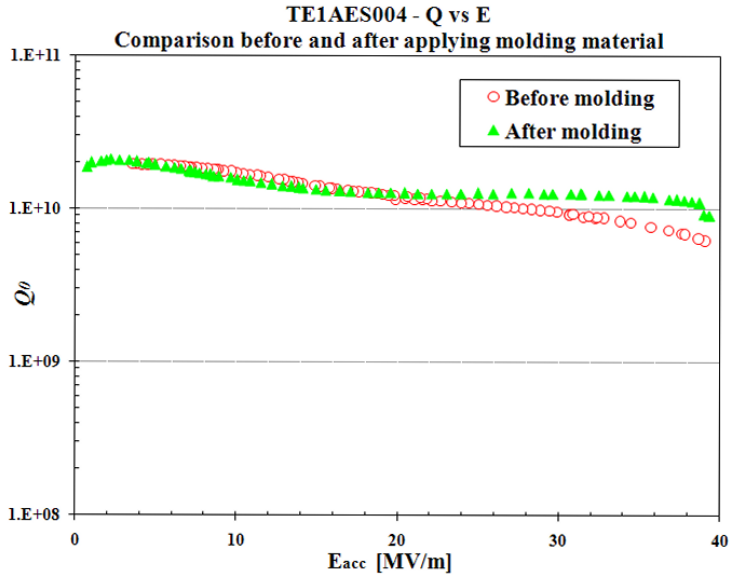

Figure 3. Cavity TE1AES004 RF performance comparisons before and after applying moulding material.

3. Examples of Cavity Surface Features

During optical inspection of cavities, many features were found; one often-seen feature is the so-called "cat eye" which corresponds to a bowl-shaped pit [5]. Replicas of the same features were analyzed with a stylus profilometer to produce 3-D surfaces. Line contours were also generated for the central contours of features. The surface plots are interpolations using a 1024 × 1024 mesh from an area profile scan recorded over 4 hours.

Four new area features were identified during the development of this replica technique: deep equator pits, a pit with a tiny peak in the middle, bumps in the EB weld path, and crevices on an iris. All the features that were replicated, except the one on a cavity iris region, caused a cavity quench.

One feature, identified as a pit, was found in the 1.3 GHz 9-cell cavity TB9ACC017. The cavity quenched at 12.3 MV/m after receiving 150 µm material removal by electropolishing. Temperature sensors confirmed that the defect location exhibited the highest temperature during the quench event at 2 K. The 3-D surface plot scanned on the replica (Figure 4-b) reveals the feature is a 140 µm deep and 200 µm diameter pit (Figure 4c and 4d). This depth-to-width ratio of 0.7 is much larger than what is typically seen for cavity pits, ~0.1 [5]. The pit is in the weld path, close to the edge of the re-solidified region, as shown in Figure 4a. The edge of the pit was indeed quite sharp, suggesting significant local field enhancement could have been possible during the RF test.

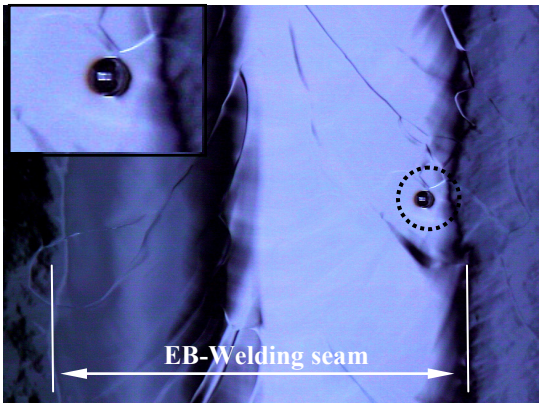

A. Inspection image of the feature in 1.3GHz 9-cell TB9ACC017 Cell #4 equator region

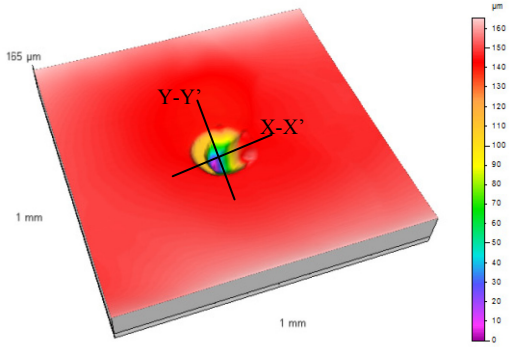

B. Surface profilometry scanned on Replica.

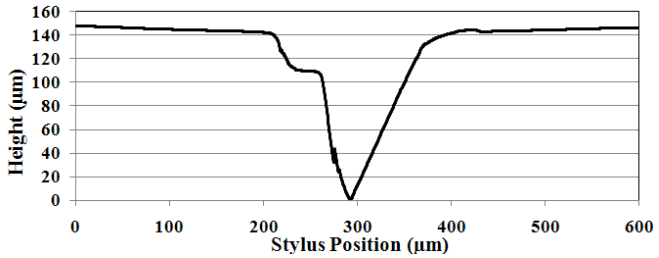

C. Line contour from X-X'

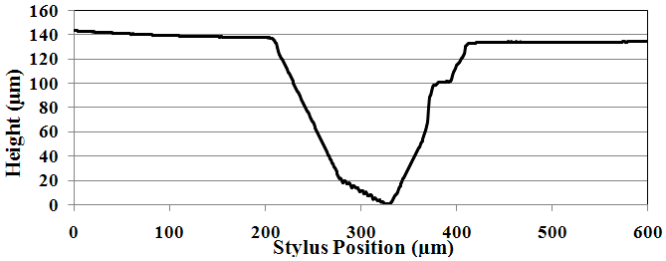

D. Line contour from Y-Y'

Figure 4. Image and profiles of a pit in 1.3 GHz 9-cell SRF cavity TB9ACC017 Cell #4 equator region. Boundaries of the weld bead are indicated on the image in (A), the inset photograph shows a magnified view of the pit. (B) is the surface plot after profilometry scanning on replica, the path in (B) used to acquire the contour profile shown at centre. At bottom (C) and (D) is the line contour.

In a 1.3 GHz single-cell SRF cavity TE1AES004, a large feature was observed near the equator electron-beam (EB) weld. The cavity received buffered chemical polishing to remove 107 µm of niobium, followed by 65 µm removed by electropolishing. The gradient went to 39 MV/m before the cavity quenched. Figure 5 shows cavity the optical inspection image and replica profilometry. In Figure 5a, the large feature located beside the welding seam is shown. In figures 5b and 5c, profilometry is shown that reveals an overall bowl shape to the pit but with a tiny peak in the center. The depth was 60 µm and diameter is 1300 µm, and the rather gradual rounding of the edges of the pit makes it difficult to conclude that the origin of field enhancement was indeed the rim of the pit. By contrast, figure 5d shows the central peak height to be 15 µm and diameter ~280 µm, with fairly abrupt curvature. It is plausible that this central feature could, in fact, be the origin of the heating that led to cavity quench. This inference could not have been made without the added information from the replica technique.

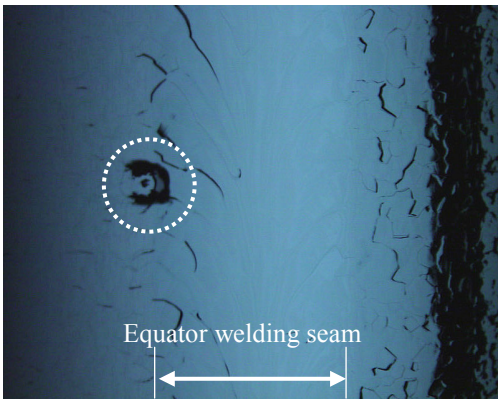

A. Inspection image of the features in 1.3 GHz single-cell cavity TE1AES004 equator region.

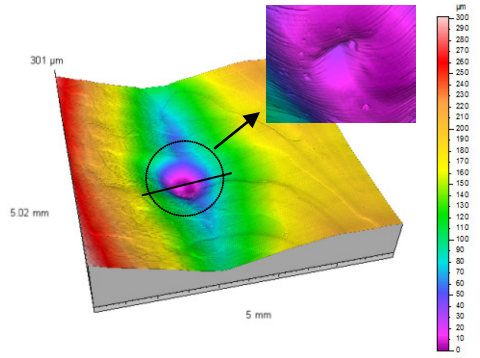

B. Surface profilometry scanned on Replica.

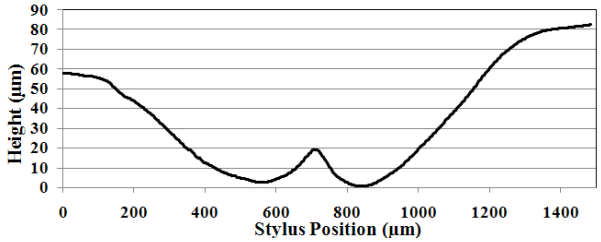

C. Line contour for Pit

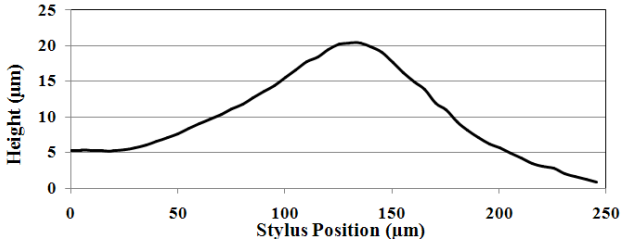

D. Line contour for the tiny peak in the center of the pit.

Figure 5. Image and profiles for cavity TE1AES004. Details described for figure 4 apply here as well. The inset photograph in (B) shows a magnified view of the tiny bump inside the pit. (D) is the line contour of the tiny bump.

Cavity TA9AES001 was also examined. This is a 1.3 GHz 9-cell cavity dressed with its helium jacket, demonstrating that replica techniques can be applied far down the processing stream. This cavity is well known for the twin large features, shown in Figure 6a, which were among the first ever confirmed by optical inspection techniques [19, 20]. The cavity received several electropolishing procedures with a total material removal of 269 µm. During numerous vertical tests, this cavity quenched at gradients between 15-21 MV/m and this obstacle has never been overcome. Replica data, Figure 6b, shows that the defects are not pits but in

fact are twin peaks. Spot (a) is 160 µm high and 700 µm in diameter; while spot (b) is 155 µm in height and 1 mm in diameter, as detailed by the line scans in Figure 6c and 6d. This new information is important in two ways. First, the defects now appear to be the result of weld spit, which could have been caused by any of several events. Second, the lack of improvement with continued etching seems reasonable given that the defect height is far too much to be removed by electropolishing. Instead, local grinding could be a reasonable repair route.

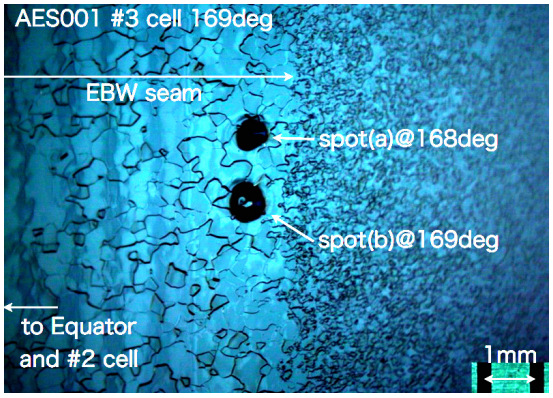

A. Inspection image of the features in 1.3 GHz 9-cell TA9AES001 Cell #3 equator region.

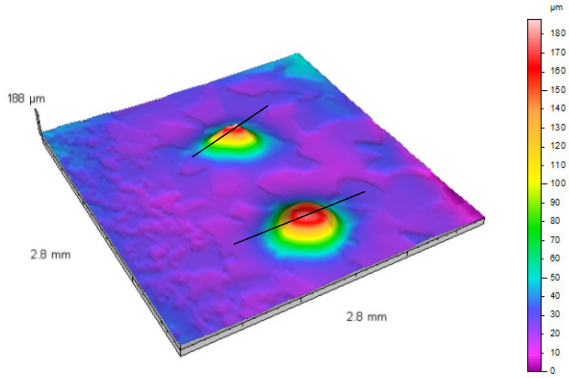

B. Surface profilometry scanned on Replica.

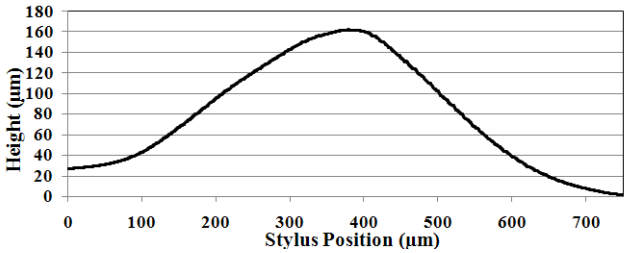

C. Line contour for Spot (a)

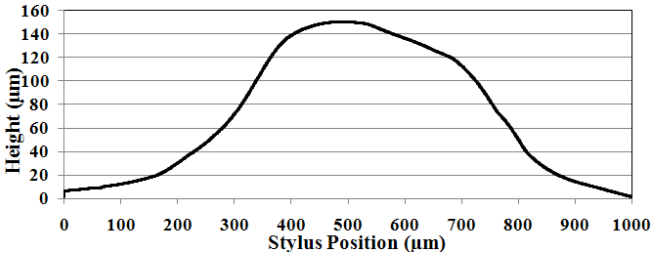

D. Line contour for Spot (b)

Figure 6. Image and profiles of twin peaks in 1.3 GHz 9-cell dressed cavity TA9AES001 Cell #3 equator region. Details described for figure 4 apply here as well.

Next, we looked at several iris features that were found in 1.3 GHz 9-cell cavity TB9JL002, as shown in Figure 7a. This replica was obtained by using the iris moulding technique discussed earlier. The geometric contour of one of these features, Figures 7b and 7c, indicates that a deep crevice extends along the bottom of the pit. While this cavity achieved 31 MV/m, it experienced strong field emission, perhaps due to this defect since the electric fields on the cavity surface are highest in the iris regions.

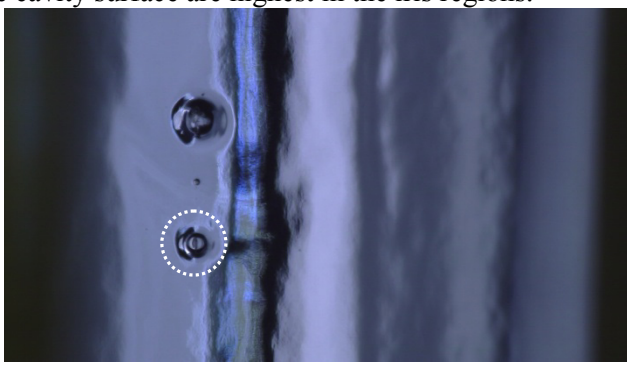

A. Optical image of several features on iris between cell #2-#3 of cavity.

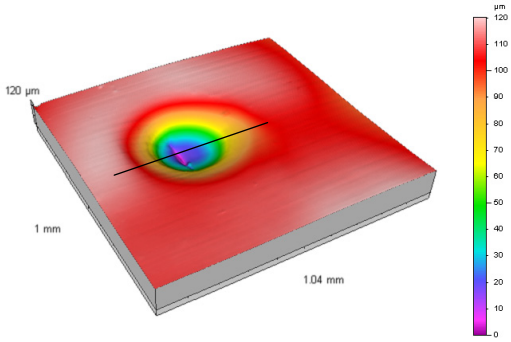

B. The 3D profile of one iris feature showing a crevice in the bottom of the deep pit.

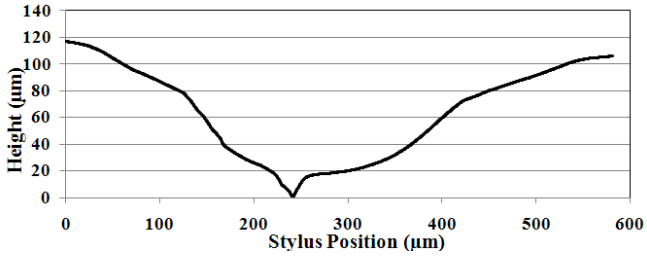

C. The line contour of center of the feature.

Figure 7. Image and profiles of pits in 1.3 GHz 9-cell TB9JL002 Cell #2-#3 iris region. Details described for figure 4 apply here as well.

4. Discussion

We demonstrate that the replica technique can be routinely applied on all kinds of SRF cavities. The extraction tool and the procedures developed at Fermilab are simple, can be easily duplicated by all SRF laboratories, and can be used in large-scale SRF activities. By using this technique, we successfully extracted surface defect 3-D profiles located in cavity equator and iris region from single-cell cavity, 9-cell

cavity, and even a 9-cell cavity fully dressed with helium jacket. These results dramatically expanded our vision and understanding of surface defects, which optical inspection technique is insufficient to reveal.

Clearly, a great amount of topographical detail was obtained without cutting pieces from SRF cavities. In addition, this technique is an ideal medium for preserving such details after each surface processing step. Topographical information can be readily obtained for as-received cavities as well as after each chemical processing step. By tracking this information, it becomes possible to more quantitatively understand how processing alters surface features. Besides gross defects at welds, which we have focused on here, sampling of cavity roughness can be compared against the parameters chosen for the chemical polishing run as a metric of quality. Feedback of roughness data could then help improve overall control and reproducibility of chemical processing.

Replicas show that most features observed by optical inspection are bowl-shaped pits. While some have very sharp contours, many have relatively smooth contours. Figure 8 is the pit profile comparison between cavity TE1AES004 and TB9ACC017 in a 1:1 scale plot. The deep pit in cavity TB9ACC017 is not typical and has much sharper rim than the more typical pit in TE1AES004. Hence the field enhancement factor at the rim of the TB9ACC017 pit is much higher than for the pit in TE1AES004 based on [9], and this difference is indeed borne out in vertical test results, where cavity TB9ACC017 reached 12 MV/m, much lower than 39 MV/m for TE1AES004. However, a completely quantitative description requires further development of models. Along this line of thinking, subtle features revealed by replicas, such as the tiny peak in figure 5 and the crevice in figure 7, should be taken into account by quench models. As it stands, the particular locations that initiate quench, whether rim or centre substructure, remains unclear. Replica data could provide sufficient information to carry out more detailed mathematical analyses on 3-D shapes, which is one area of future research at Fermilab.

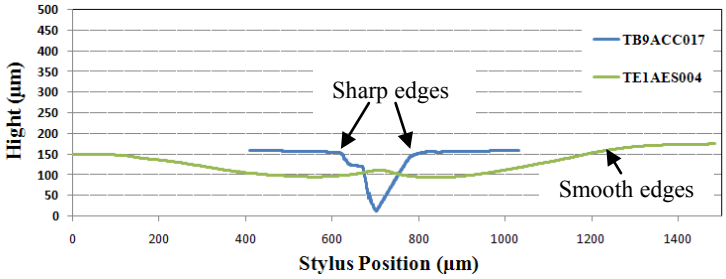

Figure 8. Profile comparison

Replicas are also useful for removing ambiguity in optical inspection. Replicas clearly distinguished bumps (figure 6) from pits. However, in the optical inspection images, they look alike. Changing the illumination direction in optical inspection attempts to gain topographical information by comparing shadows [5]. More advanced tools, such as stereoscopic imaging, in-cavity confocal microscopy or laser interferometer, or the application of digital image analysis, might eventually permit the extraction of topographical data directly from cavities. Until then, replicas will be the primary source of non-destructive topography information.

The replica findings provide clues that link specific features to imperfections in manufacture, especially electron-beam welding (EBW). All the features in the present study were located near welds and the heat affected zone. The bumps suggest Nb spatters onto the cavity surface during the welding. Perhaps this is blow-out due to improper machining or the vaporization of debris. A crevice inside a pit is evidence of incomplete welding penetration. All these data are important to improve the quality of manufacture and reduce surface defects, thus increasing the reproducibility of cavity performance.

The replica findings also provide guidance to materials science by raising questions about how defects were formed. Here, the EBW heating and cooling process combined with electrochemistry could be detrimental. For example, bubbles could be trapped underneath the surface, and re-opened by electropolishing. Pores, dislocations, and impurities are all driven along the thermal gradient of the weld and could coalesce at the edge of the heat-affected zone. Some of the pores formed during EBW could become enlarged rather than removed by electropolishing, resulting in the smooth bowl shapes commonly seen. In

other cases, tangles of dislocations could create a central core along which etching occurs at a faster pace than elsewhere on the cavity surface, leaving a tell-tale peak behind after much material has been removed. As topographical statistics are built up and combined with other analyses, mechanisms of defect formation should become easier to understand and eventually prevent.

5. Conclusion

Features such as pits or bumps were successfully characterized by a replica technique on 1.3 GHz 9-cell and 1-cell SRF cavities. Surface replicas were able to be made not only for cavity equator regions, but also at the iris region. The accuracy of this technique is micrometer scale, a resolution much smaller than the size of features seen in many SRF cavities by optical inspection systems. The 3-D surface plot and line-scan profiles reveal a wealth of topographic details that have not been discernable by other means. All the features we found were located on or near welds, some of which limited cavity RF performance to as low as 12 MV/m. The application of the replicas, followed by routine high-pressure rinsing with ultrapure water, did not change the cavity performance. Thus, this replica technique dramatically extends the visual capability of optical inspections, providing a significant amount of information about the interior surface of SRF cavities, all while preserving cavity RF performance.

Acknowledgments

Work supported by the U.S. Department of Energy under contract number DE-AC02-07CH11359. We would like to thank C Baker, D Bice, S Gerbick, and M Kelley for assistance with cavity processing. We also thank M Carter, D Massengill, and W Muranyi for cavity testing assistance. We gratefully acknowledge scientific discussions with C Antoine, Z Conway, C Cooper, and H Padamsee.

References

[1] ILC reference design report: Volume III Accelerator, P 157 (Published online at http://ilcdoc.linearcollider.org/record/6321/files/ILC_RDR_Volume_3-Accelerator.pdf?ln=en).

[2] C Ginsburg, 2010 Global Cavity Database and Yield Evaluation, *TTC meeting 2010*, (Published online at http://indico.fnal.gov/materialDisplay.py?contribId=36&sessionId=16&materialId=slides&confId=3000).

[3] Saito K, Inoue H, Kako E, Fujino T, Noguchi S, Ono M, and Shishido T 1998 Superiority of electropolishing over chemical polishing on high gradients *Particle Accelerators* **60** 193.

[4] Lilje L, Kako E, Kostin D, Matheisen A, Möller W-D, Proch D, Reschke D, Saito K, Schmüser P, Simrock S, Suzuki T, and Twarowski K 2004 Achievement of 35 MV/m in the superconducting nine-cell cavities for TESLA *Nucl. Instrum. Meth. Phys. Res. A* **524** 21.

[5] Wantanabe K 2009 Review of optical inspection methods and results *Proc. SRF 2009 (Berlin, Germany)* paper TUOBAU01 (published online at http://accelconf.web.cern.ch/accelconf/SRF2009/papers/tuobau01.pdf).

[6] Iwashita Y, Tajima Y, and Hayano H 2008 Development of high resolution camera for observations of superconducting cavities *Phys. Rev. ST Accel. Beams* **11** 093501.

[7] Knobloch J, Muller H, and Padamsee H 1994 Design of a high speed, high resolution thermometry system for 1.5 GHz superconducting radio frequency cavities *Rev. Sci. Instrum.* **65** 3521.

[8] Canabal A, Bowyer J D, Chacon P, Gillespie N A, Madrid M A, and Tajima T 2007 Development of a temperature mapping system for 1.3-GHz 9-cell SRF cavities, in *Proceedings of PAC07*, Albuquerque, New Mexico, USA (unpublished online archive at https://accelconf.web.cern.ch/accelconf/p07/PAPERS/WEPMS031.PDF).

[9] V. Shemelin, H. Padamsee, "Magnetic field enhancement at pits and bumps on the surface of superconducting cavities", TTC-Report 2008-07, (2008).

[10] Champion M, Cooley L D, Ginsburg C M, Sergatskov D A, Geng R L, Hayano H, Iwashita Y, and Tajima Y 2009 Quench-limited SRF cavities: Failure at the heat-affected zone *IEEE Trans. Appl. Supercond.* **19** 1384.

[11] Möller W-D 2009 Review of results from temperature mapping and subsequent cavity inspection *Proc. SRF 2009 (Berlin, Germany)* Paper TUOAAU04 (published online at http://accelconf.web.cern.ch/AccelConf/SRF2009/papers/tuo au04.pdf).

[12] Romanenko A, Eremeev G, Meidlinger D, and Padamsee H 2007 Studies of the high field anomalous losses in small and large grain niobium cavities *Proc. 13th Intl. Wkshp. On RF Superconductivity (Beijing, China)* paper TUP24 (published online at http://accelconf.web.cern.ch/accelconf/srf2007/PAPERS/TUP24.pdf).

[13] Romanenko A and Padamsee H 2007 Comparative surface studies on large grain and single crystal niobium using XPS, Auger, EBSD and profilometry *Proc. of PAC'07, (Albuquerque NM, USA)* p. 2349 (published online at http://accelconf.web.cern.ch/Accelconf/p07/PAPES/WEPMS011.PDF).

[14] Berry S, Antoine C, Aspart A, Charrier J P, Desmons M, and Margueritte L 2003 Topologic analysis of samples and cavities: A new tool for morphologic inspection of quench site *Proc. 11th Workshop on RF Superconductivity* (publish online at http://srf.desy.de/fap/paper/ThP04.pdf)
[15] Berry S, Antoine C, and Desmons M 2004 Surface morphology at the quench site, *Proc. of the 2004 European Particle Accelerator Conference* (published online at https://accelconf.web.cern.ch/accelconf/e04/PAPERS/TUPKF018.PDF).
[16] L. Nilsson, R. Ohlsson, 2001 Accuracy of replica materials when measuring engineering surfaces, *International Journal of Machine Tools & Manufacture* **41**, *p 2139-2145*.
[17] RTV-3040 specification (archived online at http://www.sunbeltmaterials.com/V-3040%200307%20BS.pdf).
[18] K.Watanabe, *et al*. Replica by molding and local grinding repair for 9-cell cavity. *TTC meeting 2010*, (Published online at http://indico.fnal.gov/materialDisplay.py?contribId=127&sessionId=3&materialId=slides&confId=3000)
[19] Y. Yamamoto, *et al*. Recent status of new vertical test system in KEK-STF. *TTC meeting 2010*, (Published online at http://tdserver1.fnal.gov/project/ILC/S0/9cellSummaries/TE9AES001/Yamamoto-TTC2008_India_STF_T-mapping_report_2.pdf)
[20] Y.Tajima 2008 AES001 Inspection Report (archived online at http://tdserver1.fnal.gov/project/ILC/S0/CavityHistories/AES001/report080107.pdf)